



# Corrosion Inhibition of L-Methionine Amino Acid as a Green Corrosion Inhibitor for Stainless Steel in the H<sub>2</sub>SO<sub>4</sub> Solution

M. Yeganeh, I. Khosravi-Bigdeli, M. Eskandari, and S.R. Alavi Zaree

(Submitted August 30, 2019; in revised form May 9, 2020; published online June 15, 2020)

This study investigated the effect of L-methionine (LMT) on the corrosion behavior of AISI309S stainless steel in 1 M H<sub>2</sub>SO<sub>4</sub> solution using electrochemical impedance spectroscopy (EIS), Tafel polarization, and electrochemical noise methods. The performance of corrosion inhibition was analyzed by scanning electron microscopy, atomic force microscopy, adsorption isotherms, x-ray photoelectron spectroscopy (XPS), and contact angle measurement. The electrochemical studies revealed a significant increase in the charge transfer resistance and a reduction in the corrosion current density in the presence of LMT in the acidic media. The results of the EIS and Tafel tests determined the corrosion inhibition efficiency to be about 97% and 95%, respectively. The microscopy analysis showed that the surface suffered lower corrosion damages in the presence of LMT. Besides, the adsorption of LMT on the anodic sites of the surface through its sulfur atom was verified by EIS and XPS studies.

**Keywords** 309S stainless steel, corrosion inhibitor, L-Methionine (LMT)

## 1. Introduction

The application of corrosion inhibitors is among the most effective, practical, and economical techniques for protecting metals and alloys in various corrosive media (Ref 1, 2). However, a large number of conventional corrosion inhibitors show high toxicity and are hazardous to health, including chromates, nitrite, and aromatic heterocyclic compounds. Therefore, eco-friendly inhibitors are highly recommended for corrosion protection (Ref 3-6). Natural products extract from the plant sources (Ref 1-5) and also several non-toxic organic compounds containing polar functional groups with nitrogen, oxygen and/or sulfur in their molecules have been effectively applied as inhibitors in many systems exposed to corrosion (Ref 4, 5). However, some of these compounds are ineffective at higher temperatures (Ref 6). Amino acid compounds are considered as the popular green corrosion inhibitors because they are non-toxic, biodegradable, and low cost, as well as being soluble in aqueous media (Ref 5, 7-9). Amino acid molecules have at least one carboxyl (-COOH) group and one amino (-NH<sub>2</sub>) group, which are usually bonded to the same carbon atom. In physiological media, twenty different kinds of amino acids exist, which form proteins. The presence of heteroatoms (e.g., S, N, and O) and conjugated  $\pi$ -electron systems on their molecules are the main reasons for their potential use as eco-friendly corrosion inhibitors (Ref 10).

Amino acids have been widely applied as corrosion inhibitors in many applications (Ref 11). There are several studies regarding the capability of amino acids for preventing corrosion in the case of iron (Ref 12, 13), steel (Ref 14, 15), aluminum (Ref 16, 17), nickel (Ref 18, 19), copper (Ref 20, 21), and Cu-Ni (Ref 22, 23). The amino acid methionine [CH<sub>3</sub>-S-CH<sub>2</sub>-CH<sub>2</sub>-CH(CO<sub>2</sub>H)NH<sub>2</sub>] has also been shown to be an excellent corrosion inhibitor (Ref 24). Its high inhibition efficiency can be linked to the presence of the S atom, which enhances its binding to the surface of metals. This molecule contains both (-NH<sub>2</sub>) and (-S-CH<sub>3</sub>) groups (Ref 13). The mechanism of the corrosion inhibition is based on the adsorption of the amino acid on the active sites of metals and/or the deposition of corrosion products with the formation of a 3-D layer on the surface of metals. The inhibition efficiency depends on the behavior of this layer, the configuration of the amino acid compounds, and the state of the surface (Ref 15, 22).

Austenitic stainless steel has a wide range of applications in various chemical industries due to its toughness, plasticity, and excellent corrosion properties in aqueous environments (Ref 25). Stainless steel (SS) alloys are extensively used in various industrial applications such as chemical manufacturing, food processing, and oil refining industries. Generally, stainless steel alloys are more corrosion resistant compared to ordinary steels when exposed to an acid solution (Ref 26). A few reports in the literature have focused on the corrosion protection of stainless steel by applying amino acid compounds. Ghanyl et al. (Ref 25) studied the inhibition effect of four amino acid compounds on the corrosion behavior of 316L stainless steel in 1 M H<sub>2</sub>SO<sub>4</sub>. In this study, glycine, leucine, and valine were able to inhibit the corrosion damage, while the application of arginine accelerated the corrosion rate of stainless steel. Their results showed that a high concentration of arginine led to the electrochemical activation of surface and might dissolve the passivation layer, leading to an increase in the anodic dissolution of the steel (Ref 25). Silva et al. (Ref 27) investigated the effect of cysteine on the corrosion behavior of 304L stainless steel. According to their report, high concentrations of

M. Yeganeh, I. Khosravi-Bigdeli, M. Eskandari, and S.R. Alavi Zaree, Department of Materials Science and Engineering, Faculty of Engineering, Shahid Chamran University of Ahvaz, Ahvaz, Iran. Contact e-mail: sr.alavizaree@scu.ac.ir.

cysteine led to the higher electrochemical activation of the surface of 304L stainless steel, which possibly dissolved the passivation layer and promoted the anodic dissolution of the stainless steel (Ref 27). Madkour et al. (Ref 28) evaluated the corrosion inhibition of 16/14 austenitic stainless steel by several amino acid molecules in a hydrochloric acid solution. Polarization curves revealed that the transpassive zone shifted toward more positive potentials in the presence of the amino acid, which indicated greater stability of passive film in the acidic media (Ref 28).

Corrosion behavior of 309S stainless steel in an acidic media was rarely studied so far (Ref 29-32). 309S stainless steel shows more resistance in the chemical plant and welding when compared to the conventional 304 types. It also possesses acceptable mechanical properties and corrosion resistance due to its higher Cr (~ 23 wt.%) and Ni (~ 13 wt.%) content (Ref 29). Gharbi et al. (Ref 32) studied corrosion inhibition of AISI309 austenitic stainless steel by 2,2'-bipyridyl in 0.5 M H<sub>2</sub>SO<sub>4</sub> at 298 K using different electrochemical methods. They found that the maximum inhibition efficiency was 87.78% with 10<sup>-4</sup> M of inhibitor. The obtained results confirmed the adsorption of inhibitor molecules on the surface of 309 stainless steel.

In the present work, authors have studied the corrosion inhibition of AISI309S austenitic stainless steel by the addition of L-methionine in 1 M H<sub>2</sub>SO<sub>4</sub>. The corrosion behavior was investigated using potentiodynamic polarization (Tafel), electrochemical impedance spectroscopy (EIS), and electrochemical noise methods. Besides, the characterization of samples has been performed by scanning electron microscopy (SEM), energy-dispersive spectroscopy (EDS), x-ray diffraction (XRD), x-ray photoelectron spectroscopy (XPS), and atomic force microscopy (AFM).

## 2. Materials and Methods

309S stainless steel plates (composition in wt.%, Fe: 97.7, C: 0.0617, Si: 0.46, Mn: 1.03, Cr: 22.66, Ni: 13.4, P: 0.0152, S < 0.0002, and Fe: balance) were cut to the dimension of 40 mm × 20 mm with a thickness of 3 mm. These samples were sanded with silicon carbide sandpapers (up to 1200 grit size), degreased in acetone, washed in distilled water, and dried in cold air. The L-methionine amino acid (LMT) powder was purchased from BioShop Canada Inc. The analytical grade of the sulfuric acid (H<sub>2</sub>SO<sub>4</sub>, Merck, 35-37%) was diluted with distilled water to obtain 1 M H<sub>2</sub>SO<sub>4</sub>. The solutions were prepared with an LMT concentration of 0, 50, 100 (low concentrations), 400 (medium concentration), and 700 ppm (high concentration) to study their effect on the corrosion resistance of 309S stainless steel.

All of the electrochemical studies were conducted using a three-electrode cell. In this cell, a Pt wire and an Ag/AgCl were utilized as a counter electrode and a reference electrode, respectively. A 309S stainless steel plate with an exposed area of 1 cm<sup>2</sup> was employed as the working electrode. For this aim, the sample was coated with a 3:1 mixture of beeswax and colophony resin. The electrochemical experiments were performed with an AUTOLAB PGSTAT 302 potentiostat that was controlled by NOVA software. The EIS measurements were taken at stable OCP with an amplitude of 10 mV in a frequency range of 10 kHz to 10 mHz. The ZView 3.1 software was

employed to analyze the results of the EIS by applying equivalent circuits. Additionally, the EIS tests were performed from the cathodic to the anodic potentials for the non-containing and containing LMT solutions (700 ppm) to find the mechanism of corrosion inhibition at different potentials. The potentiodynamic polarization curves were recorded by sweeping the electrode potential from -250 to +250 mV versus Ag/AgCl with a scan rate of 1 mV s<sup>-1</sup>. Tafel extrapolation method was used to obtain the polarization parameters such as corrosion current density (*i*<sub>corr</sub>), corrosion potential (*E*<sub>corr</sub>), and cathodic and anodic slopes ( $\beta_c$  and  $\beta_a$ ). Moreover, the electrochemical noise (EN) analysis was conducted in 1 M H<sub>2</sub>SO<sub>4</sub> in the presence and absence of 700 ppm of LMT, while two identical working electrodes of stainless steel and an Ag/AgCl reference electrode were immersed in the solution. The reference electrode was placed at an equal distance between the two working electrodes in the H<sub>2</sub>SO<sub>4</sub> solution. The potential and current noise data in the time domain were transformed to the frequency domain using the fast Fourier transform (FFT). Hann window function was applied to draw the power spectral density (PSD) of the data obtained by FFT. The electrochemical tests were repeated at least three times to ensure data reproducibility.

The surface morphology of the as-received and the corroded 309S stainless steel plates was analyzed using an optical microscopy (Meijitechno IM7200) and a field emission scanning electron microscope (Camscan Mira Model). The elemental distribution of oxygen and sulfur was also examined with the EDS detector. The x-ray diffraction pattern was recorded using an X'Pert Pro MPD diffractometer with monochromatic CuK $\alpha$  ( $\lambda = 1.5406 \text{ \AA}$ ) radiation in the  $2\theta$  range of 40°-80°. The surface topography and roughness average (*R*<sub>a</sub>) of 309S stainless steel plates were examined after 1 h of immersion in the 1 M solution of H<sub>2</sub>SO<sub>4</sub> without and with 700 ppm of LMT using an atomic force microscope (Nanosurf Flex model). The scanning area was set to a dimension of 10  $\mu\text{m} \times 10 \mu\text{m}$ . X-ray photoelectron spectroscopy (XPS) with an Al K anode at the energy of 1486.6 eV was applied to investigate the chemical state of 309S stainless steel after immersion in the solution containing 700 ppm LMT. The pressure of the ultra-high vacuum with  $1 \times 10^{-7}$  Pa was employed in the chamber for surface analysis. The values of the binding energy were determined by calibrating and fixing the C (1s) line to 285.0 eV content. The contact angle of the samples immersed in the H<sub>2</sub>SO<sub>4</sub> solution was measured by an optical contact angle measuring device (Data physics OCA15 plus).

## 3. Results and Discussion

Figure 1(a) and (b) shows the microstructure and x-ray pattern of 309S stainless steel, respectively. Figure 1(a) presents the optical micrograph of the as-received plate, which is composed of the austenite (96.5%) and delta ferrite (3.5%) phases. The effects of the  $\delta$ -ferrite phase on the corrosion resistance of austenitic stainless steel can be explained by the formation of a Cr-depleted zone, low concentrations of Cr and Mo in the  $\gamma$  phase, and the segregation of sulfur or phosphorus along with the austenite and ferrite interface (Ref 33). Based on literature reports, a higher delta ferrite content (5.61 wt.%) leads to the sensitization of stainless steel due to the precipitation of harmful phases (Ref 34). The  $\delta$ -ferrite phase, which is

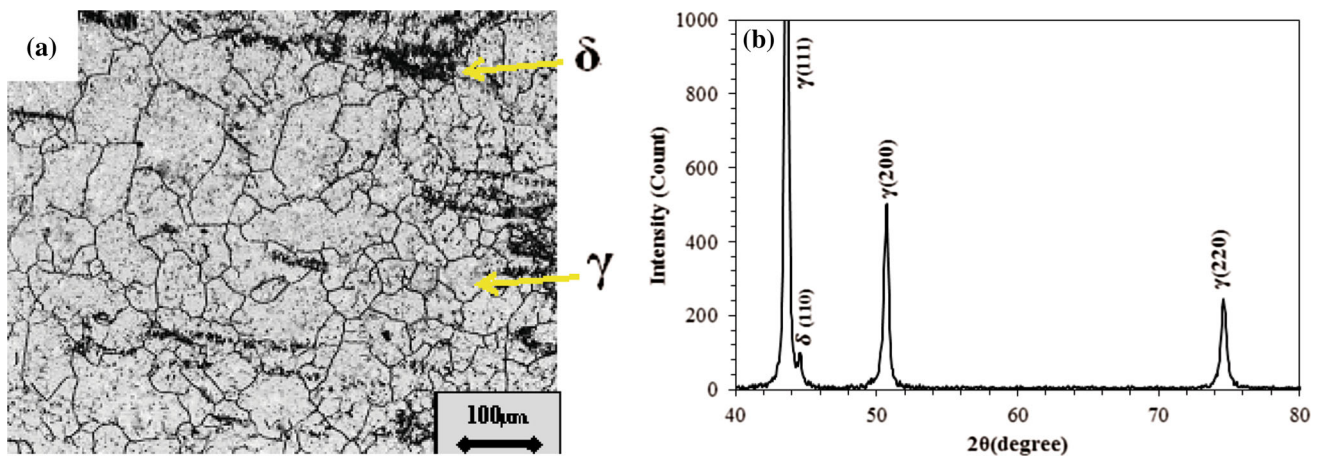


**Fig. 1** (a) Optical micrograph and (b) x-ray diffraction pattern of as-received 309S stainless steel

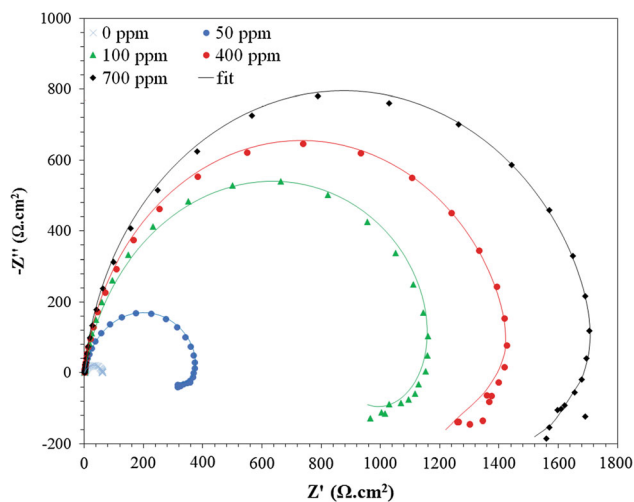


**Fig. 2** Nyquist plots for corrosion of 309S stainless steels after 1 h of immersion in 1 M  $\text{H}_2\text{SO}_4$  solution without and with different concentrations of LMT

shown as a dark phase in Fig. 1(a), is probably formed at the early stages of solidification. The average grain size of austenite in the as-received specimen is  $115 \pm 10 \mu\text{m}$ . The XRD pattern of the as-received specimen is shown in Fig. 1(b), which confirms the presence of  $\gamma$ -austenite or  $\delta$ -ferrite phase.

The corrosion behavior of the stainless steel immersed in 1 M  $\text{H}_2\text{SO}_4$  for 1 h containing LMT was studied using electrochemical impedance spectroscopy technique. Figure 2 shows Nyquist plots with their fits, which illustrate the effect of LMT on the corrosion behavior of stainless steel in the  $\text{H}_2\text{SO}_4$  solution. These curves consist of a single semicircle at the higher frequencies and a “pseudo-inductive” loop at the lower values. The capacitive loop is related to the charge transfer resistance process, while the appearance of the pseudo-inductive loop can be explained by the relaxation of adsorption species such as  $(\text{SO}_4^{2-})_{\text{ads}}$  and  $(\text{H}^+)_{\text{ads}}$  on the surface of the electrode. It can also be related to the re-dissolution of the passivated surface (Ref 35, 36). According to the Nyquist plots, the diameter of the semicircle increases when LMT is added to the  $\text{H}_2\text{SO}_4$  solution, which is probably due to the inhibition performance of LMT. The diameter of the capacitive loop in the

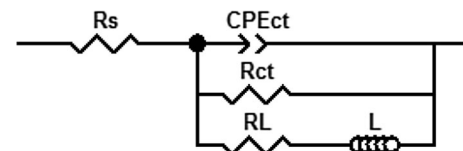


**Fig. 3** Equivalent circuit corresponding to the corrosion phenomenon at interface of 309S stainless steel without and with LMT in the  $\text{H}_2\text{SO}_4$  solution

presence of LMT is larger than in the absence of LMT. This shows that there is an increase in the charge transfer resistance, which is in agreement with the literature (Ref 35, 37). The improvement in the resistance by increasing the inhibitor concentration is a sign of high LMT-molecule adsorption on the surface of the mild steel, indicating the effective block of the surface (Ref 38).

The ZView3 software was used for evaluating the impedance data. These data were fitted according to an equivalent circuit, as presented in Fig. 3. The elements related to this circuit consist of a solution resistance,  $R_s$ , a charge transfer resistance,  $R_{ct}$ , a constant phase element, CPE, and an inductance,  $L$ .  $R_s$  is the resistance of the solution between the reference and the working electrodes, and  $R_{ct}$  represents the charge transfer resistance at the metal/electrolyte interface. Moreover,  $R_{ct}$  value is the diameter of the capacitive loop, which is directly proportional to the corrosion resistance.  $R_{ct}$  can be expressed as the value corresponding to  $Z'$  (real impedance) when  $Z''$  (imaginary impedance) = 0, which is acquired at intermediate frequencies.  $L$  is the inductance and corresponds to the low-frequency inductive loop. The appearance of inductance in the EIS plots is mainly due to the adsorbed or desorbed intermediates or other species on the surface of the electrode (Ref 39). In this study, CPE has been used instead of a pure capacitance ( $C$ ) to consider the non-ideal capacitive response of the interface. The impedance of a CPE is equal to  $A^{-1} (i \omega)^{-n}$ . Here,  $A$  is a constant related to the interfacial capacitance,  $i$  is an imaginary number,  $\omega$  is the angular frequency, and  $n$  is an exponential factor between  $-1$  and  $1$ . CPE can show resistance ( $n = 0, A = R$ ), capacitance ( $n = 1, A = C$ ), inductance ( $n = -1, A = L$ ), and Warburg impedance ( $n = 0.5, A = W$ ) depending on the value of  $n$ . Pure capacitance behavior is indicated by  $n = 1$ , while  $n$  often ranges

**Table 1 EIS parameters for the corrosion of 309S stainless steel immersed in the 1 M H<sub>2</sub>SO<sub>4</sub> without and with different concentrations of LMT after 1 h of immersion**

Inhibitor concentration	$R_s, \Omega \text{ cm}^2$	$R_{ct}, \Omega \text{ cm}^2$	$CPE_{ct}, \mu\text{F cm}^{-2}$	$R_L, \Omega \text{ cm}^2$	$L, \text{H cm}^2$	IE, %
0	1.7	54	250	235	540	...
50	1.73	382	140	1347	6499	85
100	2.14	1184	73	4367	25,216	95
400	1.39	1465	69	6500	45,022	96
700	1.88	1750	61	8053	78,872	97

from 0 to 1 in practice (Ref 39, 40).  $L$  and  $R_L$  are, respectively, the inductance ( $\text{H cm}^2$ ) and inductive resistance ( $\Omega \text{ cm}^2$ ). The values of the corrosion parameters related to the blank and the inhibitor-containing H<sub>2</sub>SO<sub>4</sub> solutions with different concentrations are presented in Table 1. Charge transfer resistance changes from 54 to 1750  $\Omega \text{ cm}^2$  as the LMT concentration increases from 0 to 700 ppm. Also, CPE-T of the uninhibited sample is higher than the amount of CPE-T related to the inhibited specimens. For instance, the value of CPE-T for the LMT-free solution and the 700 ppm LMT-containing solution is 250 and 61  $\mu\text{F cm}^{-2}$ , respectively. These changes in the value of CPE-T illustrate the adsorption of LMT on the stainless steel, which is accompanied by an increase in the thickness of the electrical double layer (capacitance  $R d^{-1}$ ) (Ref 35). The adsorption of a higher amount of LMT can result in the greater accumulation of this molecule (higher thickness  $d$ ) and leads to a lower amount of capacitance. Also, by changing the LMT concentration from 50 to 700 ppm,  $L$  and  $R_L$  change from 6499 to 78872  $\text{H cm}^2$  and 1347 to 8035  $\Omega \text{ cm}^2$ , respectively. These are noticeably higher than  $L = 540 \text{ H cm}^2$  and  $R_L = 235 \Omega \text{ cm}^2$  for the solution without LMT.

As the concentration of the inhibitor increases, the value of the charge transfer resistance becomes greater, which indicates the improved adsorption of the LMT molecule on the surface of the mild steel and leads to effective blocking on the surface (Ref 38). According to Eq 1, the inhibition efficiency (IE%) was calculated based on the impedance data by comparing the values related to the charge transfer resistance with and without LMT (Ref 38):

$$IE\% = \frac{R_{ct}^{inh} - R_{ct}}{R_{ct}^{inh}} \times 100 \quad (\text{Eq 1})$$

where  $R_{ct}^{inh}$  and  $R_{ct}$  are the inhibited and uninhibited charge transfer resistance, respectively.

The values of IE% for different concentrations of LMT are presented in Table 1. According to this table, IE% increases from 85 to 97% for 50 and 700 ppm LMT in the H<sub>2</sub>SO<sub>4</sub> solution, respectively. The inhibition efficiency is optimized with methionine (IE% = 97) for 700 ppm of LMT. The basis of the inhibition process is the adsorption of the amino acid molecules on the active sites and/or deposition of corrosion products on the surface of metal (Ref 41).

The potentiodynamic polarization measurements were taken in 1 M H<sub>2</sub>SO<sub>4</sub> in the presence or absence of LMT, as shown in Fig. 4. It is evident that in all the experiments, the polarization curves included two active zones in which the hydrogen evolution and iron dissolution reactions occurred in the cathodic and anodic sides, respectively (Ref 35). Also, both the cathodic and anodic reactions of the steel were inhibited

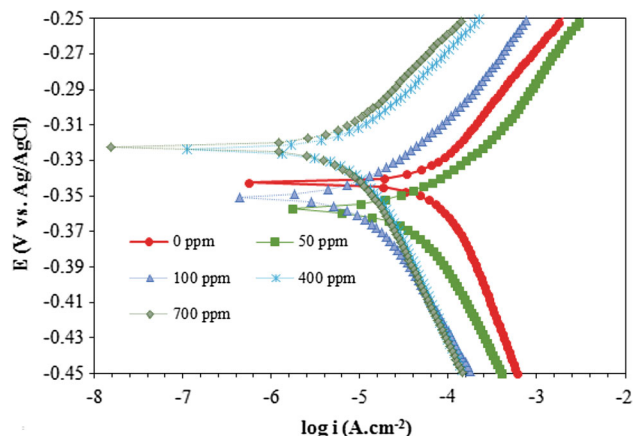


**Fig. 4** Tafel polarization curves related to the corrosion of 309S stainless steel in 1 M H<sub>2</sub>SO<sub>4</sub> in the absence and presence of LMT

when LMT was added to the acidic solution. Methionine with concentrations higher than 50 ppm could limit both the cathodic and anodic reactions. The addition of methionine could assist in reducing the anodic dissolution of iron and also postpone the hydrogen evolution reaction. Tafel lines with almost equal slopes were observed, which emphasized that the hydrogen evolution reaction was controlled by the activation process. The stability of the cathodic slope might be a sign that the mechanism of the proton discharge reaction did not change with the addition of methionine to the H<sub>2</sub>SO<sub>4</sub> solution (Ref 5).

Table 2 summarizes the estimated corrosion potential ( $E_{corr}$ ), corrosion current density ( $i_{corr}$ ), and Tafel slopes ( $\beta_a$  and  $\beta_c$ ) which were obtained using Tafel extrapolation method. According to this table, the corrosion current density in the absence of LMT was 103  $\mu\text{A cm}^{-2}$ . However, the  $i_{corr}$  values in the presence of 50-700 ppm LMT reduced from 46 to 5  $\mu\text{A cm}^{-2}$ . The lower  $i_{corr}$  showed that the surface was covered with a higher amount of corrosion inhibitor and, therefore, better performance in the H<sub>2</sub>SO<sub>4</sub> solution was observed. The corrosion potential moved toward the cathodic direction for an LMT of 50 and 100 ppm, while a shift in the anodic direction was observed for an LMT of 400 and 700 ppm in comparison with the uninhibited specimen. The most considerable potential shift was observed when 700 ppm of LMT was added to the H<sub>2</sub>SO<sub>4</sub> solution. This behavior revealed the changes in the mass and charge transfer reactions by the addition of LMT (Ref 35). In other words, the adsorption of LMT on the surface of the alloy hindered the dissolution of elements and limited the mass transfer at the interface. The inhibitor can be considered as a mixed-type inhibitor if the movement of the  $E_{corr}$  becomes lower than 85 mV in the

**Table 2 Potentiodynamic polarization parameters for the corrosion of the stainless steel in 1 M H<sub>2</sub>SO<sub>4</sub> without and with different concentrations of LMT**

Inhibitor concentration	$i_{\text{corr}}$ , $\mu\text{A cm}^{-2}$	$E_{\text{corr}}$ , mV versus Ag/AgCl	$\beta_{\text{c}}$ , mV dec <sup>-1</sup>	$\beta_{\text{a}}$ , mV dec <sup>-1</sup>	IE, %
0	103	- 339	52	38	...
50	46	- 357	50	41	55
100	12	- 351	48	40	88
400	7	- 323	52	39	93
700	5	- 321	51	40	95

absence and presence of a corrosion inhibitor. Otherwise, the corrosion inhibitor could be regarded as an anodic or a cathodic class (Ref 35, 42, 43). In the present study, the maximum observed shift in the value of  $E_{\text{corr}}$  was 21 mV toward the anodic region, which was recorded for the solution with 700 ppm of LMT, which indicated the mixed-type nature of the inhibitor with anodic tendency (Ref 44). As can be observed, the addition of 700 ppm of LMT resulted in a higher difference in the anodic potentials compared to an uninhibited sample, indicating a lower corrosion rate. Additionally, the formation of the LMT layer on the surface of the stainless steel samples could reduce the hydrogen evolution and the electron transfer at the interface of the stainless steel/H<sub>2</sub>SO<sub>4</sub> solution by increasing the charge transfer resistance and reducing the double-layer capacitance.

The inhibition efficiency (IE%) based on the  $i_{\text{corr}}$  values is calculated from Eq 2:

$$\text{IE}\% = \frac{i_{\text{corr}}^0 - i_{\text{corr}}^{\text{inh}}}{i_{\text{corr}}^0} \times 100 \quad (\text{Eq 2})$$

where  $i_{\text{corr}}^{\text{inh}}$  and  $i_{\text{corr}}^0$  are the inhibited and uninhibited corrosion current densities, respectively. It is obvious that the  $i_{\text{corr}}$  values decrease when methionine is added to the solution. In this regard, the inhibition efficiency reaches a maximum value of 95% that relates to the solution containing 700 ppm of LMT. As the inhibition efficiency increases with the addition of the inhibitor, a larger number of LMT molecules are adsorbed on the surface of the metal, leading to the higher coverage of the surface (Ref 41).

Figure 5(a) and (b) shows the EIS spectrum in the absence (a, c) and presence (b, d) of LMT (700 ppm) in the H<sub>2</sub>SO<sub>4</sub> solution with different applied cathodic or anodic potentials. The high-frequency region of the Bode and phase angle plots describes the behavior of an inhomogeneous surface layer, whereas the low-frequency region presents the charge transfer reaction phenomenon (Ref 45, 46). As can be observed in these figures, impedance modulus and phase angle increase by sweeping the potentials toward the anodic regions. The impedance modulus increases about one order of magnitude (from 2.1 to 61.3  $\Omega \text{ cm}^2$ ) in the absence of LMT, while it increases more than two orders of magnitude (from 131 to 15,100  $\Omega \text{ cm}^2$ ) in the presence of 700 ppm of LMT. It is believed that the increase in potential in the vicinity of OCP can help to provide diffusion layers of soluble reactant or product species (Ref 47, 48). The maximum phase angle increases from 4° to 52° in the absence of LMT. However, its value changes from 65° to 69° in the presence of 700 ppm of LMT. The possibility of the formation of the ferrous layer increases by sweeping the potential toward the anodic direction. Therefore,

the likelihood of the adsorption of the LMT increases from its negative site on the positive ferrous species. As mentioned before, the LMT possesses an anodic tendency at higher concentrations. The greater values of the impedance modulus and phase angle of the sample exposed to the solution containing 700 ppm of LMT compared to the uninhibited samples can be explained by the adsorption of LMT at these potentials.

Figure 6 presents CPE versus potential, which was obtained from EIS measurements of the stainless steel in the 1 M H<sub>2</sub>SO<sub>4</sub> containing 700 ppm of LMT. The value of the double-layer capacitance ( $C_{\text{dl}}$ ) is calculated using Eq 3 (Ref 45):

$$C_{\text{dl}} = \frac{1}{2\pi \cdot f_{\text{max}} \cdot R_{\text{ct}}} \quad (\text{Eq 3})$$

where  $f_{\text{max}}$  is the frequency at the highest imaginary impedance and  $R_{\text{ct}}$  is charge transfer resistance.  $R_{\text{ct}}$  could be substituted by the impedance modulus at some anodic potentials related to 700 ppm of LMT. The EIS data in each potential were extracted and transferred to this plot.

The potential of zero charge (PZC) plays a crucial role in the electrostatic adsorption of the species. The ac impedance study was carried out to evaluate the potential of zero charge (Ref 49). The Antropov's rational corrosion potential ( $E_r$ ), which is the electrode potential in a reduced scale, could be expressed by the potential of zero charge ( $E_{\text{PZC}}$ ) of the same electrode and can be calculated by Eq 4 (Ref 50):

$$E_r = E_{\text{OCP}} - E_{\text{PZC}} \quad (\text{Eq 4})$$

In the present study,  $E_r$  is calculated as + 229 mV, which shows the positive charging of 309S stainless steel in 1 M H<sub>2</sub>SO<sub>4</sub> solution in the presence of 700 ppm of LMT. It is most probable that the inhibitor molecules can be directly adsorbed on the stainless steel surface by the electrostatic interactions between the positively charged metal surface and the anionic portion of the inhibitor molecules. The inhibitive action of the LMT in the H<sub>2</sub>SO<sub>4</sub> solution can be explained by the physical adsorption of the negatively charged LMT to the positively charged surface, forming a barrier layer on it. The charge sharing or transfer between the  $d$  orbitals of the metal and LMT molecules can take place after the adsorption of the LMT on the surface. The chemical adsorption of the inhibitor molecules is also a result of the donor-acceptor interactions taking place between the free electron pairs of the N, S, and O atoms, as well as the  $\pi$  electrons of the multiple bonds and empty  $d$  orbitals of the metal (Ref 51). The quantum chemical evaluations reveal that the LMT molecules are noticeably able to exchange electrons with the metal surface (Ref 5). On the other hand, the adsorption of methionine through the positively charged

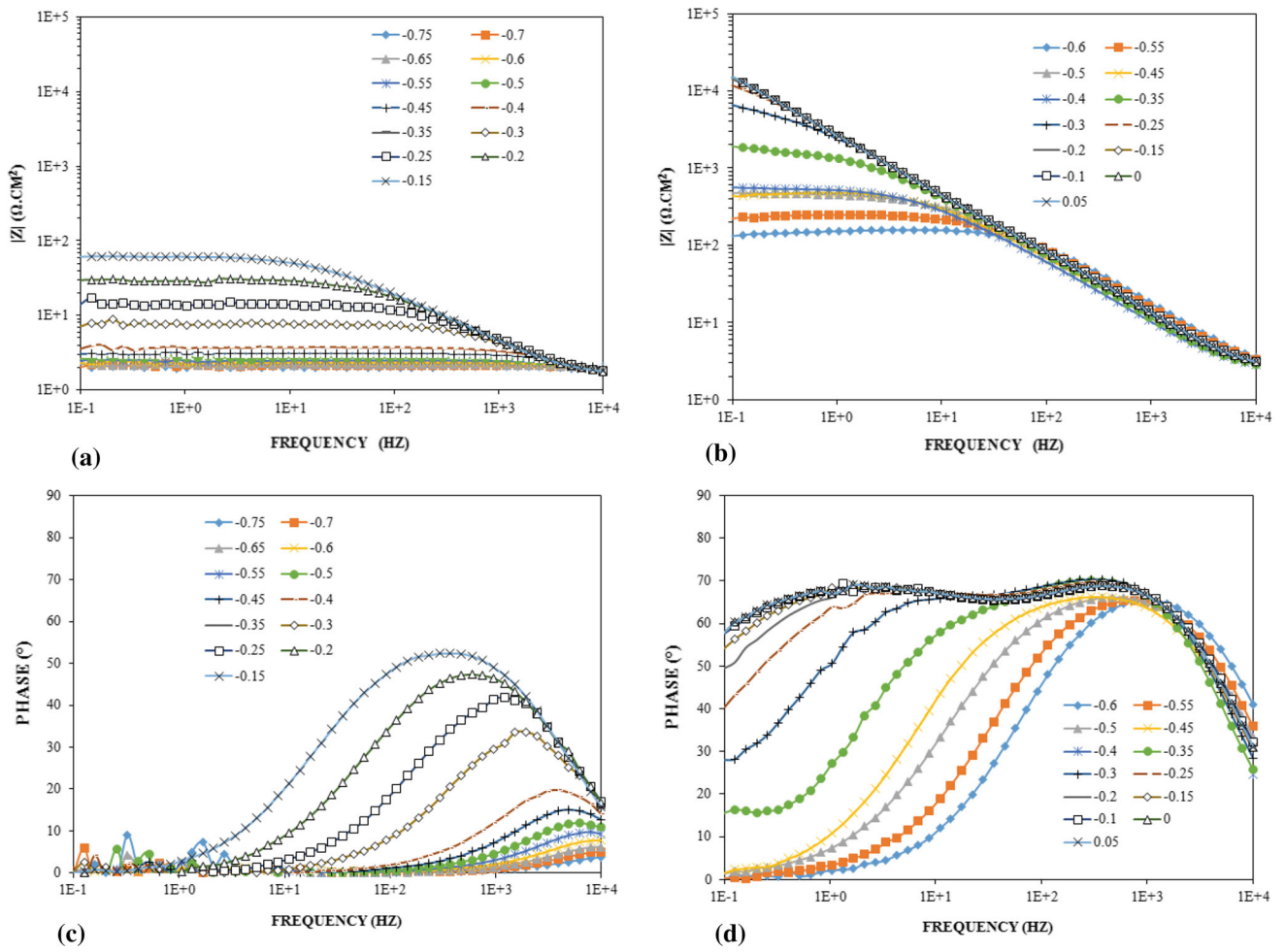


**Fig. 5** EIS plots related to the corrosion of 309S stainless steel in 1 M H<sub>2</sub>SO<sub>4</sub> in the absence (a and c) and presence (b and d) of 700 ppm of LMT at different potentials

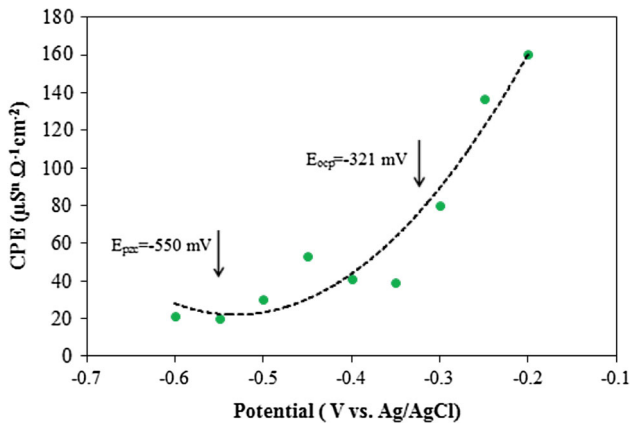


**Fig. 6** Capacitance vs. potential plot recorded for 309S stainless steel electrode in 1 M H<sub>2</sub>SO<sub>4</sub> solution containing 700 ppm of LMT

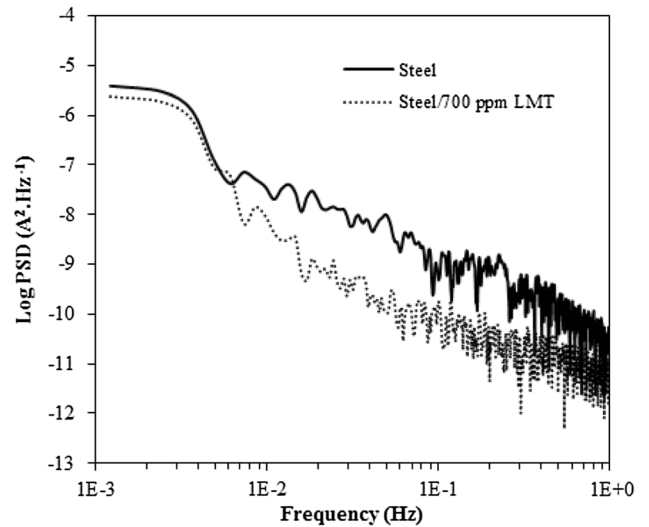


**Fig. 7** Power spectral density (PSD) of current for the steel and the steel/700 ppm LMT measured in 1 M H<sub>2</sub>SO<sub>4</sub> solution

nitrogen atom may not occur most probably due to the presence of a positive charge on the surface of the steel in the H<sub>2</sub>SO<sub>4</sub> solution, according to Eq 4. Therefore, a high degree of surface coverage is expected as a result of the adsorption of this compound at the anodic sites on the surface of stainless steel through its molecular configuration (Ref 52).

The electrochemical noise technique was also utilized to evaluate the corrosion performance of the steel immersed in the H<sub>2</sub>SO<sub>4</sub> solution containing 700 ppm of LMT. The power

spectral density (PSD) of the measured current for the stainless steel immersed in the  $H_2SO_4$  solution without and with 700 ppm of LMT is shown in Fig. 7. A lower value of PSD (I) for the steel/700 ppm LMT reveals a higher corrosion resistance due to the adsorption of the methionine molecule on the surface of the stainless steel. Furthermore, a reduction in the noise level is a sign of the lower electrochemical activity of the steel immersed in the solution containing LMT (Ref 53). Moreover, the noise resistance ( $R_n$ ), which was calculated by the ratio of the standard deviations of the voltage fluctuations to the current variations (Ref 54, 55), revealed that the corrosion resistance of the stainless steel immersed in the  $H_2SO_4$  solution containing 700 ppm of LMT was higher compared to the uninhibited sample. The calculated  $R_n$  for the steel/700 ppm

LMT was  $650 \Omega \text{ cm}^2$ , while that of the uninhibited steel was  $75 \Omega \text{ cm}^2$ . The higher resistance of the steel/700 ppm LMT could be explained by the existence of heteroatoms (e.g., S, N, and O) and conjugated  $\pi$ -electrons on the molecular structure of LMT (Ref 10).

SEM and AFM studies were conducted to investigate the surface and elemental analysis of the 309S stainless steel immersed in the acidic solution containing 700 ppm of LMT. Figure 8(a) shows that the uninhibited surface of stainless steel was attacked in the  $H_2SO_4$  solution, and several pits appeared. According to the FESEM micrographs, the surface of the sample showed a rough morphology with several pits in the absence of LMT, which reveals a corrosion attack. The surface of 309S stainless steel sample immersed in the solution

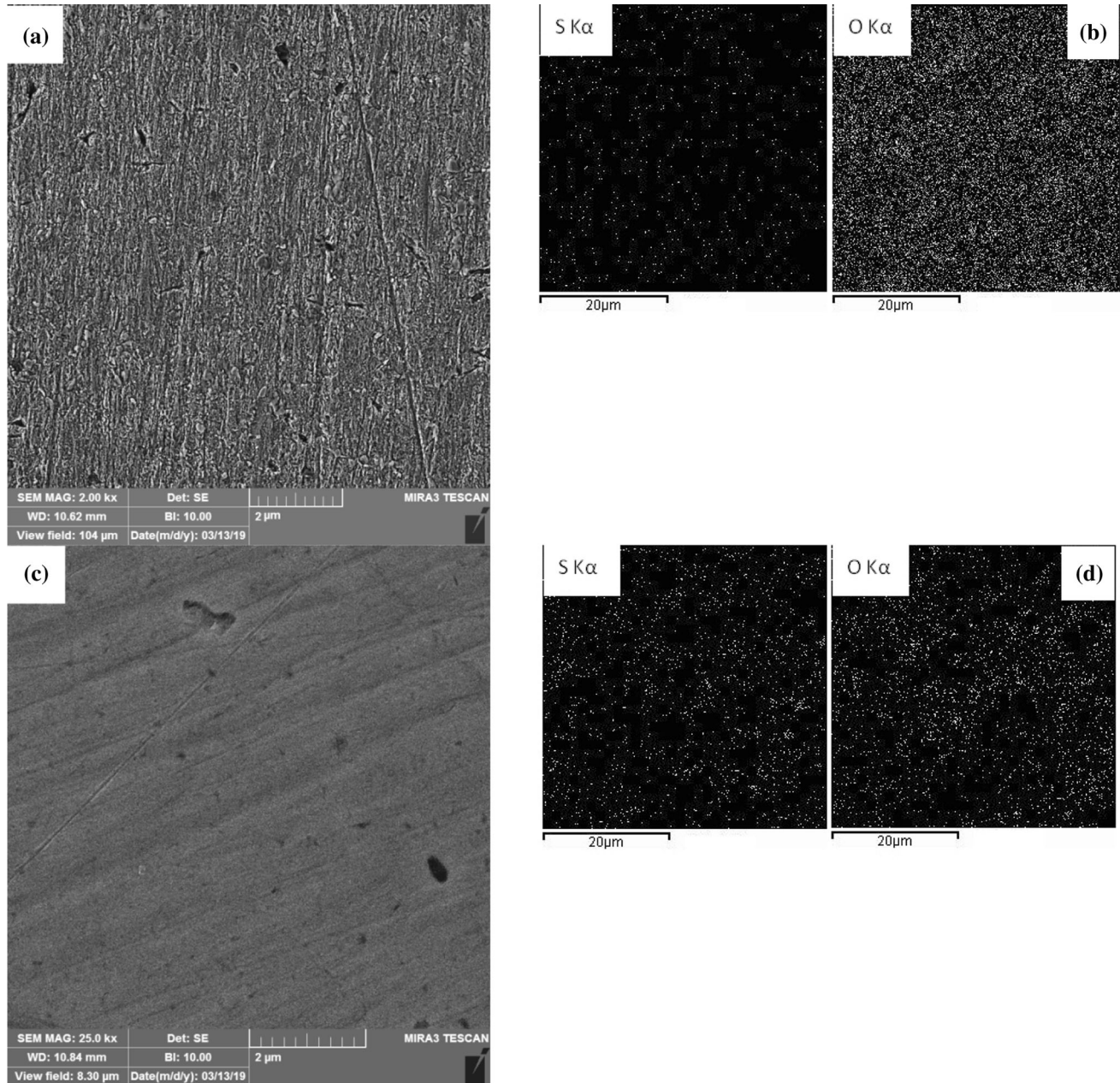


**Fig. 8** FESEM micrographs and EDS maps of (a and b): stainless steel immersed in 1 M  $H_2SO_4$  solution; (c and d) stainless steel immersed in 1 M  $H_2SO_4$  containing 700 ppm of LMT

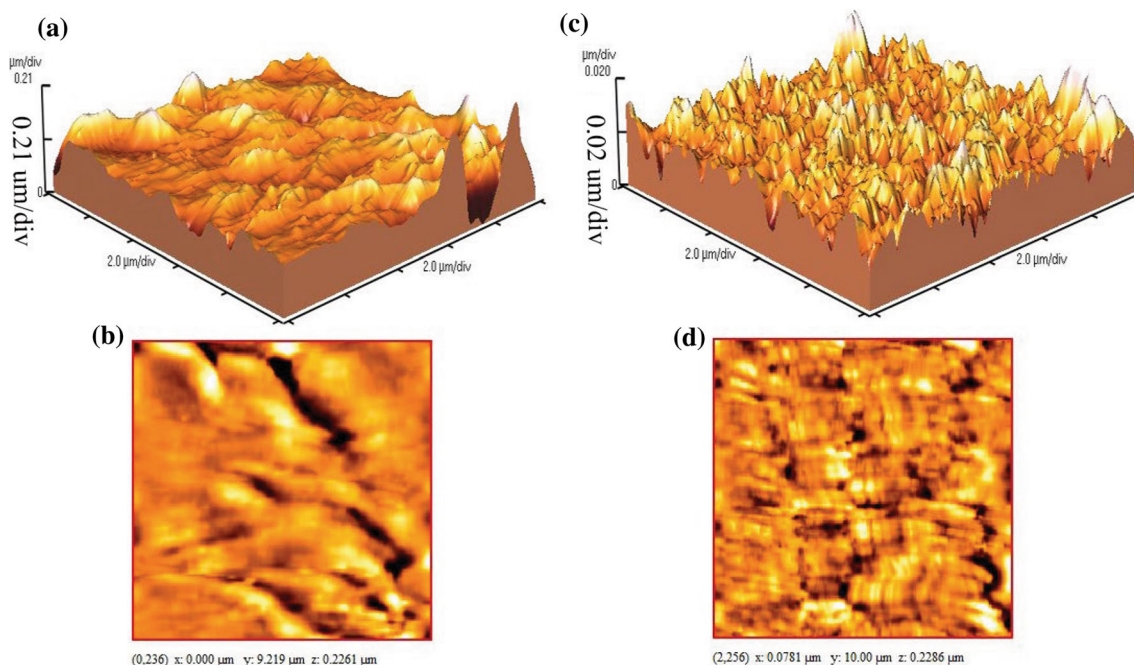


**Fig. 9** AFM surface topography of the 309S stainless steel specimens (a and b) steel immersed in 1 M H<sub>2</sub>SO<sub>4</sub> without inhibitor, (c and d) steel immersion in 1 M H<sub>2</sub>SO<sub>4</sub> in the presence of 700 ppm of LMT

containing 700 ppm of LMT suffered fewer damages than the uninhibited sample (Fig. 8c). The smooth morphology and the lower damages were observed in the presence of 700 ppm of LMT in the acidic solution. The results of EDS mapping revealed the presence of O and S on the surface of the steel. The greater value of the oxygen element corresponding to the uninhibited sample indicated the presence of higher corrosion products on the surface of the steel (Fig. 8b). On the other hand, the higher amount of detected sulfur on the sample dipped in the solution with 700 ppm of LMT confirmed the adsorption of the inhibitor molecules (C<sub>5</sub>H<sub>11</sub>NO<sub>2</sub>S) on the surface of the steel (Fig. 8d).

Atomic force microscopy was employed to evaluate the surface topography of 309S stainless steel specimens immersed in the 1 M H<sub>2</sub>SO<sub>4</sub> solution without and with 700 ppm of LMT. The AFM images and the height profiles are presented for both samples in Fig. 9. The measured *R<sub>a</sub>* value for the specimens without and with LMT was about 320 and 32 nm, respectively. This is in agreement with the literature (Ref 56, 57) and can be explained by the adsorption of LMT, which forms a protective barrier. In the presence of LMT, the corrosion resistance was enhanced, and a different surface morphology with a smoother surface was observed. The effect of the LMT inhibitor in reducing the surface roughness is in agreement with the works of other researchers (Ref 35).

Figure 10(a) and (b) shows the adsorption isotherm according to the EIS and polarization data, respectively. The data could be well fitted according to the Langmuir isotherm (Ref 58). Langmuir adsorption isotherm is presented according to Eq 5 (Ref 58):

$$\frac{C_{\text{inh}}}{\theta} = \frac{1}{K_{\text{ads}}} + C_{\text{inh}} \quad (\text{Eq 5})$$

where *C* is the concentration of the inhibitor, *K<sub>ads</sub>* is the adsorption equilibrium constant, and *θ* is the degree of surface

coverage of the inhibitor. The plot of (*C<sub>inh</sub>*/*θ*) versus *C<sub>inh</sub>* illustrates a linear relationship, as shown in Fig. 10. The parameters related to the Langmuir isotherm are provided in Table 3. If the value of *R*<sup>2</sup> is higher than 0.96, it indicates the excellent fitting of the data to the Langmuir adsorption isotherm (Ref 58). Since the experimental results are properly fitted to the Langmuir adsorption isotherm, the other adsorption isotherms have not been examined.

Another parameter that can be assessed from the adsorption isotherm is Gibb's free energy. Standard Gibb's free energy  $\Delta G_{\text{ads}}^0$  can be calculated using Eq 6 (Ref 58):

$$\Delta G_{\text{ads}}^0 = -RT \ln(55.5K_{\text{ads}}) \quad (\text{Eq 6})$$

where *R* is the gas constant and *T* is the absolute temperature. The concentration of water in the solution is 55.5 mol l<sup>-1</sup>. Generally, the value of  $\Delta G_{\text{ads}}^0$  up to -20 kJ mol<sup>-1</sup> indicates the physical adsorption arising from the electrostatic interaction between the charged inhibitor molecules and the surface of the steel, while  $\Delta G_{\text{ads}}^0$  less than -40 kJ mol<sup>-1</sup> reveals the chemical adsorption, emphasizing the sharing or transferring of the charge from the inhibitor molecule to the surface, which forms a coordinate bond (chemisorption) (Ref 59, 60). If the calculated values of  $\Delta G_{\text{ads}}^0$  stand between -20 and -40 kJ mol<sup>-1</sup>, it is supposed that the adsorption includes both physisorption and chemisorption reactions (Ref 35). As can be observed in Table 3,  $\Delta G_{\text{ads}}^0$  for the EIS and polarization tests is calculated to be -35 and -33.3 kJ mol<sup>-1</sup>, respectively. Therefore, the adsorption possesses both physisorption and chemisorption characteristics when 309S stainless steel is immersed in the H<sub>2</sub>SO<sub>4</sub> solution containing LMT.

The feasibility of a chemical reaction occurring between the methionine and the surface can be verified by XPS analysis. The spectra of the steel dipped in the 700 ppm of LMT are presented in Fig. 11(a). The figure shows that C, N, O, S, and Fe are present in this sample, which indicates the adsorption of



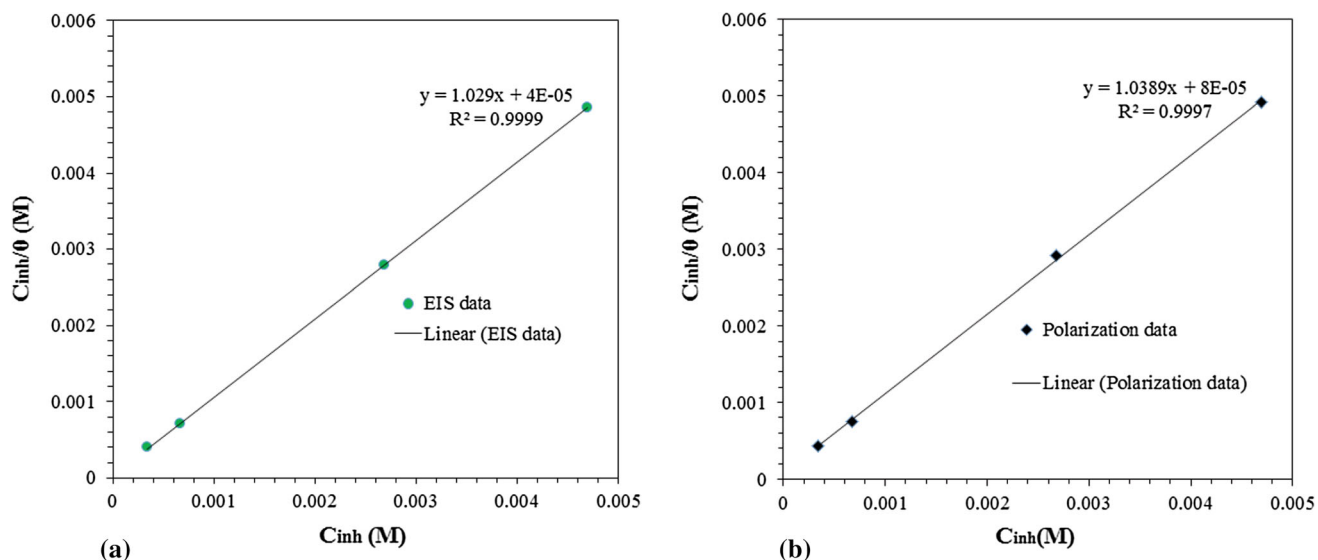


**Fig. 10** Graph of the Langmuir isotherm study calculated for the adsorption of LMT on 309S stainless steel specimens in 1 M H<sub>2</sub>SO<sub>4</sub> obtained from (a) EIS and (b) polarization data

**Table 3** Adsorption parameters calculated for the adsorption of LMT on the surface of stainless steel in 1 M H<sub>2</sub>SO<sub>4</sub> obtained from EIS and polarization tests

Obtained data	R <sup>2</sup>	K <sub>ads</sub>	ΔG <sub>0</sub> <sup>ads</sup> , kJ mol <sup>-1</sup>
EIS	0.9999	25,000	- 35
Polarization	0.9997	12,500	- 33.3

methionine on the surface. The XPS spectra of the Fe 2p<sub>3/2</sub> (Fig. 11b) reveal a broadband that emphasizes a combination of several peaks, which are the characteristics of the surface of the steel. The spectrum of the steel immersed in the solution containing LMT shows three peaks of about 707.3, 709.2, and 711.68 eV, which belong to the Fe(II)-S, Fe(III)-S, and Fe(III)-O bonds, respectively. The LMT can interact with the corroding surface of the steel via the protonated amino groups by adsorbing at the cathodic sites and hindering the hydrogen evolution; or through the sulfur atom in its molecular structure, which may adsorb at the anodic sites reducing the dissolution rate of iron (Ref 41). As mentioned in the EIS section, the adsorption of LMT would be favored during the anodic sweep of the potential, which can be explained by the enhancement of the interaction between the sulfur and the surface of the steel at the anodic potentials. The formation of FeS bonds could emphasize this behavior according to the XPS results.

Figure 12 shows the contact angle measurement of the stainless steel surfaces after dipping for 1 h in the solution in the absence or the presence of different concentrations of LMT. The results revealed an increase in the contact angle by the addition of LMT. The greatest increase in contact angle was observed in the case of 700 ppm of LMT. The contact angle increased from about 71 to 85° with the addition of the corrosion inhibitor in the solution from 0 to 700 ppm. It could be explained by an increase in the surface hydrophobicity of the samples after immersion in the solution containing LMT. The adsorption of methionine on the active site of the stainless steel

was responsible for an increase in the value of the contact angle and reduction in the corrosion damage (Ref 61).

According to the mentioned results, LMT is a mixed-type inhibitor with an anodic tendency, which inhibits the corrosion of stainless steel in 1 M H<sub>2</sub>SO<sub>4</sub> by both electrostatic (physisorption) and charge sharing (chemisorption) interactions according to Fig. 13. The adsorption of the protonated methionine on the cathodic sites on the surface of steel retards the hydrogen evolution reaction. The adsorption on the anodic sites of the surface can occur through the sulfur atom in the aliphatic chain, retarding the dissolution process of the steel. The methionine derivatives can influence both the cathodic (based on the polarization results) and anodic (based on the EIS and XPS results) reactions (Ref 5). The sulfur atoms can interact chemically with the surface of steel (according to XPS) (Ref 47), while the protonated functional groups in the methionine can provide physical bonds due to their attraction toward the surface. The amino, carbonyl, and hydroxyl groups can support the interaction between the methionine molecule and the surface of the steel (Ref 35). Finally, it can be acknowledged that the methionine molecule has the ability to adsorb on the surface of the steel via chemical and physical bonds (Fig. 13). Therefore, the addition of LMT can have a positive effect on the corrosion resistance of stainless steel in the H<sub>2</sub>SO<sub>4</sub> media.

## 4. Conclusion

In this work, methionine was suggested as an effective substance for inhibiting the corrosion of 309S stainless steel in 1 M H<sub>2</sub>SO<sub>4</sub> solution. The results showed that the corrosion resistance of the stainless steel increased noticeably from 54 to 1750 Ω cm<sup>2</sup> by increasing the concentration of LMT from 0 to 700 ppm. The maximum efficiency was 97%, as reported in the EIS tests. According to the thermodynamic calculations, the LMT was adsorbed on the surface of the specimens through

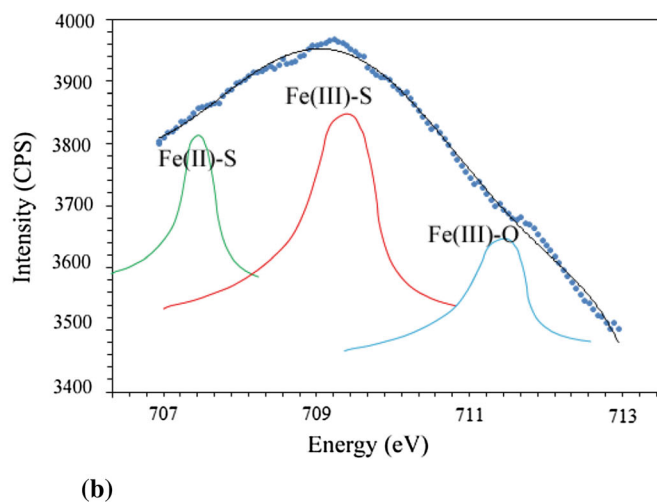
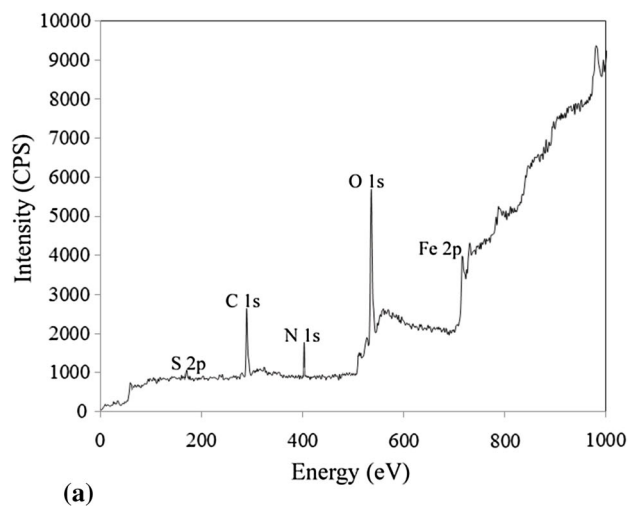


**Fig. 11** (a) XPS survey spectrum of the stainless steel surface immersed in the 700 ppm of LMT and (b) Fe ( $2p_{3/2}$ ) with the higher magnification

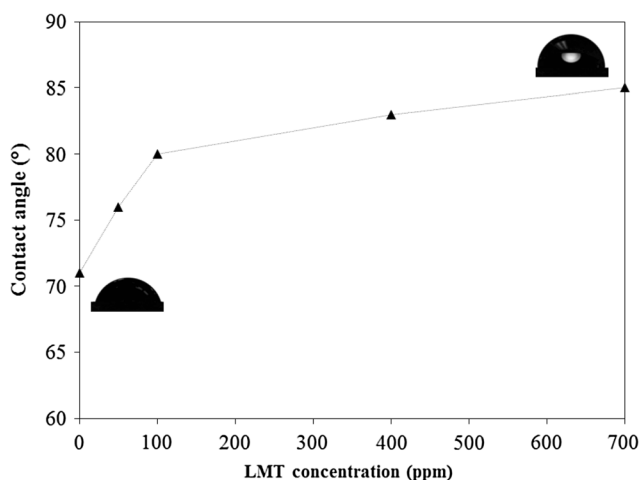


**Fig. 12** Contact angle measurement of the stainless steel after immersion in the 1 M  $H_2SO_4$  solution containing different concentrations of LMT

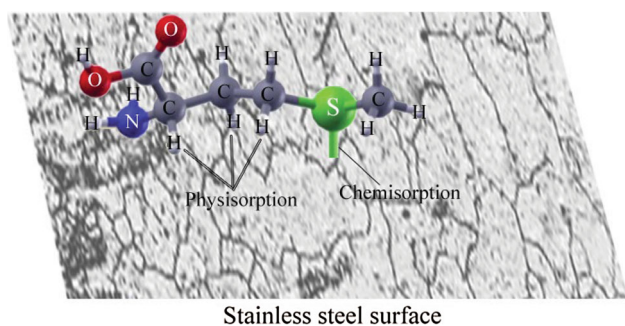


**Fig. 13** Schematic of the interactions between the LMT and the surface of stainless steel in the  $H_2SO_4$  solution

both physical and chemical adsorption processes, which was emphasized by the XPS, polarization, and EIS studies. It can be concluded that the chemical bond between the sulfur and iron led to the chemisorption process, while the interaction of the

functional groups of LMT and the surface resulted in the physisorption process.

### Acknowledgments

This research was financially supported by Shahid Chamran University of Ahvaz with the Grant Numbers of SCU.EM98.3139 and SCU.EM98.236.

### References

1. M. Mobin, M. Parveen, and M.Z.A. Rafiquee, Synergistic Effect of Sodium Dodecyl Sulfate and Cetyltrimethyl Ammonium Bromide on the Corrosion Inhibition Behavior of L-Methionine on Mild Steel in Acidic Medium, *Arab. J. Chem.*, 2017, **10**, p S1364–S1372. <https://doi.org/10.1016/j.arabjc.2013.04.006>
2. L. Hamadi, S. Mansouri, K. Oulmi, and A. Kareche, The Use of Amino Acids as Corrosion Inhibitors for Metals: A Review, *Egypt. J. Pet.*, 2018, **27**, p 1157–1165. <https://doi.org/10.1016/j.ejpe.2018.04.004>
3. J.A. Thangakani, S. Rajendran, J. Sathiyabama, R.J. Rathish, and S. Santhanaprabha, Corrosion Inhibition of Carbon Steel in Well Water by L-Cysteine-Zn<sup>2+</sup> System, *Port. Electrochim. Acta*, 2017, **35**, p 13–25. <https://doi.org/10.4152/pea.201701013>
4. M.S.S. Morad, A.E.-H.A. Hermas, and M.S. Abdel Aal, Effect of Amino Acids Containing Sulfur on the Corrosion of Mild Steel in Phosphoric Acid Solutions Polluted with Cl<sup>-</sup>, F<sup>-</sup> and Fe<sup>+3</sup> Ions—Behaviour Near and at the Corrosion Potential, *J. Chem. Technol. Biotechnol.*, 2002, **77**, p 486–494. <https://doi.org/10.1002/jctb.588>
5. K.F. Khaled, Monte Carlo Simulations of Corrosion Inhibition of Mild Steel in 0.5 M Sulphuric Acid by Some Green Corrosion Inhibitors, *J. Solid State Electrochem.*, 2009, **13**, p 1743–1756. <https://doi.org/10.1007/s10008-009-0845-y>
6. E.B. Ituen, O. Akaranta, and S.A. Umoren, N-Acetyl Cysteine Based Corrosion Inhibitor Formulations for Steel Protection in 15% HCl Solution, *J. Mol. Liq.*, 2017, **246**, p 112–118. <https://doi.org/10.1016/j.molliq.2017.09.040>
7. J.J. Fu, S.N. Li, Y. Wang, L.H. Cao, and L.D. Lu, Computational and Electrochemical Studies of Some Amino Acid Compounds as Corrosion Inhibitors for Mild Steel in Hydrochloric Acid Solution, *J. Mater. Sci.*, 2010, **45**, p 6255–6265. <https://doi.org/10.1007/s10853-010-472-0-0>
8. Z. Zhang, W. Li, W. Zhang, X. Huang, L. Ruan, and L. Wu, Experimental, Quantum Chemical Calculations and Molecular Dynamics (MD) Simulation Studies of Methionine and Valine as Corrosion Inhibitors on Carbon Steel in Phase Change Materials (PCMs)

- Solution, *J. Mol. Liq.*, 2018, **272**, p 528–538. <https://doi.org/10.1016/j.molliq.2018.09.081>
9. G.M.A. El-Hafez and W.A. Badawy, The Use of Cysteine, N-Acetyl Cysteine and Methionine as Environmentally Friendly Corrosion Inhibitors for Cu–10Al–5Ni Alloy in Neutral Chloride Solutions, *Electrochim. Acta*, 2013, **108**, p 860–866. <https://doi.org/10.1016/j.electacta.2013.06.079>
  10. B. El Ibrahim, A. Jmiai, L. Bazzi, and S. El Issami, Amino Acids and Their Derivatives as Corrosion Inhibitors for Metals and Alloys, *Arab. J. Chem.*, 2017, <https://doi.org/10.1016/j.arabjc.2017.07.013>
  11. M.S. Morad, Effect of Sulfur-Containing Amino Acids on the Corrosion of Mild Steel in Sulfide-Polluted Sulfuric Acid Solutions, *J. Appl. Electrochem.*, 2007, **37**, p 1191–1200. <https://doi.org/10.1007/s10800-007-9386-1>
  12. M.A. Amin, K.F. Khaled, Q. Mohsen, and H.A. Arida, A Study of the Inhibition of Iron Corrosion in HCl Solutions by Some Amino Acids, *Corros. Sci.*, 2010, **52**, p 1684–1695. <https://doi.org/10.1016/j.corsci.2010.01.019>
  13. M. Zerfaouia, H. Oudda, B. Hammouti, S. Kertit, and M. Benkaddour, Inhibition of Corrosion of Iron in Citric Acid Media by Amino Acids, *Prog. Org. Coat.*, 2004, **51**, p 134–138. <https://doi.org/10.1016/j.porgcoat.2004.05.005>
  14. H. Ashassi-Sorkhabi, M.R. Majidi, and K. Seyyedi, Investigation of Inhibition Effect of Some Amino Acids Against Steel Corrosion in HCl Solution, *Appl. Surf. Sci.*, 2004, **225**, p 176–185. <https://doi.org/10.1016/j.apsusc.2003.10.007>
  15. L.K.M.O. Goni, M.A.J. Mazumder, S.A. Ali, M.K. Nazal, and H.A. Al-Muallem, Biogenic Amino Acid Methionine-Based Corrosion Inhibitors of Mild Steel in Acidic Media, *Int. J. Min. Metall. Mater.*, 2019, **26**, p 467–482. <https://doi.org/10.1007/s12613-019-1754-4>
  16. A.A. El-Shafei, M.N.H. Moussa, and A.A. El-Far, Inhibitory Effect of Amino Acids on Al Pitting Corrosion in 0.1 M NaCl, *J. Appl. Electrochem.*, 1997, **27**, p 1075–1078. <https://doi.org/10.1023/A:1018490727290>
  17. C. Zhu, H.X. Yang, Y.Z. Wang, D.Q. Zhang, and Y.C.X. Gao, Synergistic Effect Between Glutamic Acid and Rare Earth Cerium (III) as Corrosion Inhibitors on AA5052 Aluminum Alloy in Neutral Chloride Medium, *Ionics*, 2019, **25**, p 1395–1406. <https://doi.org/10.1007/s11581-018-2605-4>
  18. G. Gece and S. Bilgiç, A Theoretical Study on the Inhibition Efficiencies of Some Amino Acids as Corrosion Inhibitors of Nickel, *Corros. Sci.*, 2010, **52**, p 3435–3443. <https://doi.org/10.1016/j.corsci.2010.06.015>
  19. A.A. Aksüt and S. Bilgiç, The Effect of Amino Acids on the Corrosion of Nickel in H<sub>2</sub>SO<sub>4</sub>, *Corros. Sci.*, 1992, **33**, p 379–387. [https://doi.org/10.1016/0010-938X\(92\)90067-D](https://doi.org/10.1016/0010-938X(92)90067-D)
  20. K. Barouni, L. Bazzi, R. Salghi, M. Mihit, B. Hammouti, A. Albourine, and S. El Issami, Some Amino Acids as Corrosion Inhibitors for Copper in Nitric Acid Solution, *Mater. Lett.*, 2008, **62**, p 3325–3327. <https://doi.org/10.1016/j.matlet.2008.02.068>
  21. K.F. Khaled, Corrosion Control of Copper in Nitric Acid Solutions Using Some Amino Acids—A Combined Experimental and Theoretical Study, *Corros. Sci.*, 2010, **52**, p 3225–3234. <https://doi.org/10.1016/j.corsci.2010.05.039>
  22. W.A. Badawy, K.M. Ismail, and A.M. Fathi, Corrosion Control of Cu–Ni Alloys in Neutral Chloride Solutions by Amino Acids, *Electrochim. Acta*, 2006, **51**, p 4182–4189. <https://doi.org/10.1016/j.electacta.2005.11.037>
  23. H. Saifia, M.C. Bernard, S. Joiret, K. Rahmouni, H. Takenouti, and B. Talhi, Corrosion Inhibitive Action of Cysteine on Cu–30Ni Alloy in Aerated 0.5 M H<sub>2</sub>SO<sub>4</sub>, *Mater. Chem. Phys.*, 2010, **120**, p 661–669. <https://doi.org/10.1016/j.matchemphys.2009.12.011>
  24. X. Li, W. Li, S. Yang, and L. Hou, Using Methionine as an Environment-Friendly Corrosion Inhibitor for Copper–Nickel Alloy in a Chloride Solution, *Mater. Express*, 2017, **7**, p 480–490. <https://doi.org/10.1166/mex.2017.1397>
  25. N.A. Abdel Ghanyl, A.E. El-Shenawy, and W.A.M. Hussien, The Inhibitive Effect of Some Amino Acids on the Corrosion Behaviour of 316L Stainless Steel in Sulfuric Acid Solution, *Mod. Appl. Sci.*, 2011, **5**, p 19–30. <https://doi.org/10.5539/mas.v5n4p19>
  26. S. Vikneshvaran and S. Velmathi, Adsorption of L-Tryptophan-Derived Chiral Schiff Bases on Stainless Steel Surface for the Prevention of Corrosion in Acidic Environment: Experimental, Theoretical and Surface Studies, *Surf. Interfaces*, 2017, **6**, p 134–142. <https://doi.org/10.1016/j.surf.2017.01.001>
  27. A.B. Silva, S.M.L. Agostinho, O.E. Barcia, G.G.O. Cordeiro, and E. D'Elia, The Effect of Cysteine on the Corrosion of 304L Stainless Steel in Sulphuric Acid, *Corros. Sci.*, 2006, **48**(11), p 3668–3674. <https://doi.org/10.1016/j.corsci.2006.02.003>
  28. L. Madkour and M. Ghoneim, Inhibition of the Corrosion of 16/14 Austenitic Stainless Steel by Oxygen and Nitrogen Containing Compounds, *Bull. Electrochem.*, 1997, **13**, p 1–7
  29. W. Ye, Y. Li, and F. Wang, Effects of Nanocrystallization on the Corrosion Behavior of 309 Stainless Steel, *Electrochim. Acta*, 2006, **51**, p 4426–4432. <https://doi.org/10.1016/j.electacta.2005.12.034>
  30. W. Ye, Y. Li, and F. Wang, The Improvement of the Corrosion Resistance of 309 Stainless Steel in the Transpassive Region by Nano-Crystallization, *Electrochim. Acta*, 2009, **54**, p 1339–1349. <https://doi.org/10.1016/j.electacta.2008.08.073>
  31. K. Fushimi, A. Naganuma, K. Azumi, and Y. Kawahara, Current Distribution during Galvanic Corrosion of Carbon Steel Welded with Type-309 Stainless Steel in NaCl Solution, *Corros. Sci.*, 2008, **50**, p 903–911. <https://doi.org/10.1016/j.corsci.2007.10.003>
  32. A. Gharbi, A. Himour, S. Abderrahmane, and K. Abderrahim, Inhibition Effect of 2,2'-Bipyridyl on the Corrosion of Austenitic Stainless Steel in 0.5 M H<sub>2</sub>SO<sub>4</sub>, *Orient. J. Chem.*, 2018, **34**, p 314–325. <https://doi.org/10.13005/ojc/340134>
  33. S.Y. Kim, H.S. Kwon, and H. Kim, Effect of Delta Ferrite on Corrosion Resistance of Type 316L Stainless Steel in Acidic Chloride Solution by Micro-droplet Cell, *Solid State Phenom.*, 2007, **124–126**, p 1533–1536. <https://doi.org/10.4028/www.scientific.net/SSP.124-126.1533>
  34. R.T. Loto and E. Özcan, Corrosion Resistance Studies of Austenitic Stainless Steel Grades in Molten Zinc–Aluminum Alloy Galvanizing Bath, *J. Fail. Anal. Prev.*, 2016, **16**, p 427–437. <https://doi.org/10.1007/s11668-016-0103-4>
  35. T. Rabizadeh and S. Khameneh-Asl, Casein as a Natural Protein to Inhibit the Corrosion of Mild Steel in HCl Solution, *J. Mol. Liq.*, 2019, **276**, p 694–704. <https://doi.org/10.1016/j.molliq.2018.11.162>
  36. H. Ashassi-Sorkhabi and E. Asghari, Effect of Hydrodynamic Conditions on the Inhibition Performance of L-Methionine as a “Green” Inhibitor, *Electrochim. Acta*, 2008, **54**, p 162–167. <https://doi.org/10.1016/j.electacta.2008.08.024>
  37. V. Shkirskiy, P. Keil, H. Hintze-Bruening, F. Leroux, F. Brisset, K. Ogle, and P. Volovitch, The Effects of L-Cysteine on the Inhibition and Accelerated Dissolution Processes of Zinc Metal, *Corros. Sci.*, 2015, **100**, p 101–112. <https://doi.org/10.1016/j.corsci.2015.07.010>
  38. M.A. Chidiebere, E.E. Oguzie, L. Liu, Y. Li, and F. Wang, Ascorbic Acid as Corrosion Inhibitor for Q235 Mild Steel in Acidic Environments, *J. Ind. Eng. Chem.*, 2015, **26**, p 182–192. <https://doi.org/10.1016/j.jiec.2014.11.029>
  39. M. Yeganeh, M. Omid, and M. Eskandari, Superhydrophobic Surface of AZ31 Alloy Fabricated by Chemical Treatment in the NiSO<sub>4</sub> Solution, *J. Mater. Eng. Perform.*, 2018, **27**, p 3951–3960. <https://doi.org/10.1007/s11665-018-3479-3>
  40. M. Yeganeh, M. Eskandari, and S.R. Alavi-Zaree, A Comparison Between Corrosion Behaviors of Fine-Grained and Coarse-Grained Structures of High-Mn Steel in NaCl Solution, *J. Mater. Eng. Perform.*, 2017, **26**, p 2484–2490. <https://doi.org/10.1007/s11665-017-2685-8>
  41. S. Zor, F. Kandemirli, and M. Bingu, Inhibition Effects of Methionine and Tyrosine on Corrosion of Iron in HCl Solution: Electrochemical, FTIR, and Quantum-Chemical Study, *Prot. Met. Phys. Chem. Surf.*, 2009, **45**, p 46–53
  42. K. Barouni, A. Kassale, A. Albourine, O. Jbara, B. Hammouti, and L. Bazzi, Amino Acids as Corrosion Inhibitors for Copper in Nitric Acid Medium: Experimental and Theoretical Study, *J. Mater. Environ. Sci.*, 2014, **5**, p 456–463
  43. K. Wan, P. Feng, B. Hou, and Y. Li, Enhanced Corrosion Inhibition Properties of Carboxymethyl Hydroxypropyl Chitosan for Mild Steel in 10 M HCl Solution, *RSC Adv.*, 2016, **6**, p 77515–77524. <https://doi.org/10.1039/C6RA12975G>
  44. S. Jagadeesan, P. Sounthari, K. Parameswari, and S. Chitra, Acenaphtho[1,2-b]quinoxaline and Acenaphtho[1,2-b]pyrazine as Corrosion Inhibitors for Mild Steel in Acid Medium, *Measurement*, 2015, **77**, p 175–186. <https://doi.org/10.1016/j.measurement.2015.09.008>
  45. E.E. Oguzie, Y. Li, and F.H. Wang, Corrosion Inhibition and Adsorption Behavior of Methionine on Mild Steel in Sulfuric Acid

- and Synergistic Effect of Iodide Ion, *J. Colloid Interface Sci.*, 2007, **310**, p 90–98. <https://doi.org/10.1016/j.jcis.2007.01.038>
46. M. Saremi and M. Yeganeh, Corrosion Behavior of Copper Thin Films Deposited by EB-PVD Technique on Thermally Grown Silicon Dioxide and Glass in Hydrochloric Acid Media, *Mater. Chem. Phys.*, 2010, **123**, p 456–462. <https://doi.org/10.1016/j.matchemphys.2010.04.041>
  47. D.Q. Zhang, B. Xie, L.X. Gao, H.G. Joo, and K.Y. Lee, Inhibition of Copper Corrosion in Acidic Chloride Solution by Methionine Combined with Cetrimonium Bromide/Cetylpyridinium Bromide, *J. Appl. Electrochem.*, 2011, **41**, p 491–498. <https://doi.org/10.1007/s10800-011-0259-2>
  48. M. Saremi and M. Yeganeh, Investigation of Corrosion Behaviour of Nanostructured Copper Thin Film Produced by Radio Frequency Sputtering, *Micro Nano Lett.*, 2010, **5**, p 70–75. <https://doi.org/10.1049/mnl.2009.0111>
  49. M.A. Amin, Weight Loss, Polarization, Electrochemical Impedance Spectroscopy, SEM and EDX Studies of the Corrosion Inhibition of Copper in Aerated NaCl Solutions, *J. Appl. Electrochem.*, 2006, **36**, p 215–226. <https://doi.org/10.1007/s10800-005-9055-1>
  50. R. Solmaz, Investigation of Corrosion Inhibition Mechanism and Stability of Vitamin B1 on Mild Steel in 0.5 M HCl Solution, *Corros. Sci.*, 2014, **81**, p 75–84. <https://doi.org/10.1016/j.corsci.2013.12.006>
  51. A.R. Hoseinzadeh, I. Danaee, and M.H. Maddahy, Thermodynamic and Adsorption Behaviour of Vitamin B1 as a Corrosion Inhibitor for AIS 4130 Steel Alloy in HCl Solution, *Z. Phys. Chem.*, 2013, **227**, p 403–417. <https://doi.org/10.1524/zpch.2013.0276>
  52. M. Özcan, F. Karadağ, and İ. Dehric, Investigation of Adsorption Characteristics of Methionine at Mild Steel/Sulfuric Acid Interface: An Experimental and Theoretical Study, *Colloid Surf. A Physicochem. Eng. Aspects*, 2008, **316**, p 55–61. <https://doi.org/10.1016/j.colsurfa.2007.08.023>
  53. M. Yeganeh, M. Omid, and T. Rabizadeh, Anti-corrosion Behavior of Epoxy Composite Coatings Containing Molybdate-Loaded Mesoporous Silica, *Prog. Org. Coat.*, 2019, **126**, p 18–27. <https://doi.org/10.1016/j.porgcoat.2018.10.016>
  54. R. Naderi and M.M. Attar, Effect of Zinc-Free Phosphate-Based Anticorrosion Pigment on the Cathodic Disbondment of Epoxy-Polyamide Coating, *Prog. Org. Coat.*, 2014, **77**, p 830–835
  55. B.P. Markhali, R. Naderi, M. Mahdavian, M. Sayebani, and S.Y. Arman, Electrochemical Impedance Spectroscopy and Electrochemical Noise Measurements as Tools to Evaluate Corrosion Inhibition of Azole Compounds on Stainless Steel in Acidic Media, *Corros. Sci.*, 2013, **75**, p 269–279
  56. A. Dehghani, G. Bahlakeh, B. Ramezanzadeh, and M. Ramezanzadeh, A Combined Experimental and Theoretical Study of Green Corrosion Inhibition of Mild Steel in HCl Solution by Aqueous *Citrullus lanatus* Fruit (CLF) Extract, *J. Mol. Liq.*, 2019, **279**, p 603–624. <https://doi.org/10.1016/j.molliq.2019.02.010>
  57. A. Dehghani, G. Bahlakeh, and B. Ramezanzadeh, A Detailed Electrochemical/Theoretical Exploration of the Aqueous Chinese Gooseberry Fruit Shell Extract as a Green and Cheap Corrosion Inhibitor for Mild Steel in Acidic Solution, *J. Mol. Liq.*, 2019, **282**, p 366–384. <https://doi.org/10.1016/j.molliq.2019.03.011>
  58. S.S. Abd El Rehim, S.M. Sayyah, M.M. El-Deeb, S.M. Kamal, and R.E. Azooz, Adsorption and Corrosion Inhibitive Properties of P(2-aminobenzothiazole) on Mild Steel in Hydrochloric Acid Media, *Int. J. Ind. Chem.*, 2016, <https://doi.org/10.1007/s40090-015-0065-5>
  59. N.A. Odewunmi, S.A. Umoren, and Z.M. Gasem, Utilization of Watermelon Rind Extract as a Green Corrosion Inhibitor for Mild Steel in Acidic Media, *J. Ind. Eng. Chem.*, 2015, **21**, p 239–247. <https://doi.org/10.1016/j.jiec.2014.02.030>
  60. A. Singh, K.R. Ansari, M.A. Quraishi, H. Lgaz, and Y. Lin, Synthesis and Investigation of Pyran Derivatives as Acidizing Corrosion Inhibitors for N80 Steel in Hydrochloric Acid: Theoretical and Experimental Approaches, *J. Alloys Compd.*, 2018, **762**, p 347–362. <https://doi.org/10.1016/j.jallcom.2018.05.236>
  61. N. Asadi, M. Ramezanzadeha, G. Bahlakeh, and B. Ramezanzadeh, Utilizing Lemon Balm Extract as an Effective Green Corrosion Inhibitor for Mild Steel in 1 M HCl Solution: A Detailed Experimental, Molecular Dynamics, Monte Carlo and Quantum Mechanics Study, *J. Taiwan Inst. Chem. Eng.*, 2019, **95**, p 252–272. <https://doi.org/10.1016/j.jtice.2018.07.011>

**Publisher's Note** Springer Nature remains neutral with regard to jurisdictional claims in published maps and institutional affiliations.